

Behavior of cold-formed steel shear walls sheathed with high-capacity sheathing

Fani Derveni*, Simos Gerasimidis, Kara D. Peterman

Department of Civil and Environmental Engineering, University of Massachusetts, Amherst, 130 Natural Resources Road, Amherst, MA 01003, United States

ARTICLE INFO

Keywords:

Cold-formed steel
Shear walls
Lateral force resisting systems
Computational modeling
Connection testing

ABSTRACT

Cold-formed steel (CFS) framed buildings have shown potential towards innovative and efficient building design in high seismic regions. The objective of this study is to expand the knowledge and breadth of design options of CFS construction into higher capacity lateral force resisting systems; as such, the lateral performance of CFS shear walls sheathed with fiber cement board (FCB) and composite steel-gypsum (SG) panels are the focus of this work. Three-dimensional finite element shell modeling is used by focusing on the impact of sheathing type, screw type and fastener pattern. The computational method includes fastener-based modeling which necessitates the use of experimentally-derived connection behavior. An experimental program of monotonic and cyclic fastener testing was conducted to provide shear response of CFS-to-sheathing connections with various sheathings (FCB, SG), screws, and screw spacing. Monotonic connection means are derived from the experiments and introduced in the finite element model. The numerical results demonstrate significant capacity benefits and different failure modes from traditional wood-sheathed shear walls. This work not only aims to provide an innovative and accurate computational tool for FCB- and SG-sheathed shear walls to the research community, but also to expand CFS practice through higher capacity design options. To enable adoption by practitioners, prescriptive design recommendations are provided. As the developed finite element model is computationally expensive, Pinching4 parameters from the cyclic testing are also provided to aid in the development of reduced-order models.

1. Introduction

Cold-formed steel (CFS) light gauge construction is widely adopted across North America for low-rise and mid-rise seismic applications since it is composed of lightweight, economical, durable, non-combustible and recyclable CFS components. CFS can be used for both structural and non-structural building systems, including as the designated lateral force resisting system. CFS shear walls, braced or sheathed, act as the most common lateral load resisting systems. Significant research has been conducted for CFS shear walls sheathed with wood structural panels or steel sheet and they are enabled within the AISI-S400 design specifications [1]. However, predictive capacities for CFS shear walls sheathed with cement-based or composite panels are not currently available to the designer. As shear walls sheathed with these panels can offer higher capacities and superior fire retardant performance, enabling design using these systems for the practicing engineer motivates this work.

Extensive experimental CFS shear wall studies have been conducted for oriented-strand board (OSB), plywood or gypsum sheathed CFS

shear walls under monotonic and/or cyclic loading by Santa Clara University [2], McGill University [3] and Johns Hopkins University [4]. Serrette et al. [2] investigated the impact of sheathing materials such as OSB, plywood, gypsum wallboard and proprietary panels, as well as the influence of lateral straps and fastener spacing. Branston et al. [3] was focused on OSB- and plywood-sheathed CFS shear walls, investigating the impact of perimeter sheathing fastener spacing and wall aspect ratio. Liu et al. [4] examined construction detailing through OSB- and gypsum-sheathed CFS shear wall experiments varying: wall aspect ratio, configuration of horizontal and vertical seams, presence of a ledger, field stud thickness, and presence or absence of interior gypsum panels. Steel-sheathed CFS shear walls were also experimentally investigated by Macillo et al. [5], varying steel sheathing thickness, fastener spacing and wall aspect ratio, and resulting to steel sheathing buckling and screw pull-out primary failure modes, as well as chord stud flange distortion for smaller perimeter fastener spacings. DaBreo et al. [6] additionally examined and tested the impact of CFS members thickness, framing type and loading type for steel-sheathed shear walls. The impact of corrugated steel as a cladding material was also

* Corresponding author.

E-mail address: fderveni@umass.edu (F. Derveni).

experimentally evaluated under lateral loading by Fulöp and Dubina [7] and under combined gravity and lateral loading by Zhang et al. [8]. As demand for cold-formed steel in seismic regions increases, so too does the demand for higher capacity shear walls.

Gypsum- and cement-based sheathing materials have attracted interest from researchers worldwide. Mohebbi et al. [9] tested six shear wall configurations sheathed by fiber cement board (FCB), gypsum, steel-gypsum (SG) composite, fiber cement board to steel composite and bare steel panels subjected to cyclic loading. They concluded that fiber cement board and gypsum claddings increased the strength and stiffness of steel-sheathed shear walls, while further strength and stiffness increase was predicted for double-sided claddings. Shear walls sheathed with impact resistant gypsum-based boards were experimentally investigated by Macillo et al. [10] and Fiorino et al. [11] through monotonic and cyclic wall sub-system tests and shake table (white noise and earthquake) full two-story building tests, respectively. FCB-sheathed CFS shear walls were also examined by Zeynalian and Ronagh [12] under monotonic and cyclic loading and by Khaliq and Moghish [13] under monotonic loading, while SG-sheathed CFS shear walls were tested by Hoehler et al. [14] under cyclic and fire loads, concluding that fire exposure leaded to global steel sheet failure.

Within a computational modeling framework, a variety of finite element software programs and methods have been used by the research community. Fastener-based models were attempted through both, phenomenological performance-based modeling efforts in OpenSees [15] and high fidelity modeling efforts in ABAQUS [16]. Specifically, OSB-sheathed CFS shear wall performance-based phenomenological models have been introduced under cyclic loading from Buonopane et al. [17] and Bian et al. [18] by using Pinching4 parameters for connection simulation in OpenSees. High-fidelity finite element modeling efforts have been conducted for OSB-sheathed CFS shear walls in ABAQUS by Ngo [19] through spring connection representation, Ding [20] through user-defined UEL subroutines for Pinching4 connection representation, and Derveni et al. [21] through a two-stage approach for nonlinear connector elements representation. Because fastener failures govern the wall response, fastener-based modeling is reflective of reality and accurately captures shear wall response. Steel-sheathed CFS shear walls have been also numerically approached in OpenSees Singh and Hutchinson [22] and ABAQUS Zhang and Schafer [23] through fastener-based models. Fiorino et al. [24] computationally examined the lateral performance of gypsum-based sheathed CFS shear walls via detailed FE models in SAP2000 and equivalent and unified FE truss models in OpenSees tackling different modeling approaches in comparison to previous experiments.

Since shear connection behavior is fundamental to the overall wall lateral response, significant attention has been given to their experimental response. Connection behavior between cold-formed steel studs and OSB or gypsum sheathing was investigated by Peterman et al. [25] under monotonic and cyclic loading and Pinching4 parameters were extracted from the tests. Pinching4 parameters were also obtained through single-screw testing by Tao et al. [26] for OSB, plywood, gypsum and steel sheathing to stud connections. Vieira and Schafer [27] conducted monotonic connection testing by altering fastener spacing, environmental conditions, edge distance and field procedures. Monotonic experiments were also conducted by Derveni et al. [21] through a 30-identical specimen program in an effort to quantify connection response high variability between CFS and OSB. Connections with different sheathing types, such as steel-gypsum (SG), fiber cement board (FCB), particle cement board, plywood and gypsum, as well as different stud cross-sections were tested under monotonic loading by Selvaraj and Madhavan [28]. Fiorino et al. [29] also conducted CFS-to-sheathing monotonic connection testing, for different gypsum-based and cement-based panels, thicknesses and fastener types.

Although various research efforts exist for wood- and steel-sheathed shear walls, there are limited studies considering fiber cement board (FCB) and steel-gypsum (SG) composite board as sheathing materials at

both connection and subsystem levels.

The first goal of this work is to study the lateral performance of CFS shear walls sheathed with increasingly-used FCB and SG composite panels. This study is initiated by an experimental program of 18 test specimens of CFS-to-sheathing connections to determine the shear response of the connections subjected to monotonic and cyclic loading. A hysteretic connection characterization follows and backbones and Pinching4 parameters are extracted from the tests. Based on the experimentally-obtained fastener behavior, fastener-based computational models are introduced, investigating strength, stiffness and failure modes of the examined wall configurations. The main and final focus of this study is the recommended design guidelines for these systems, as obtained from the finite element modeling framework. This work constitutes an expansion of CFS building construction capabilities and capacities and provides fundamental performance benchmarks for eventual implementation into design codes.

2. Test program of CFS-to-FCB and CFS-to-SG shear connections

Shear tests on CFS-to-sheathing connections are conducted herein for fiber cement board (FCB) and steel-gypsum composite board (SG) sheathings. This aims to provide not only shear connection capacities for effective CFS design purposes, but also extracted data for high-fidelity finite element modeling purposes.

2.1. Test assembly and test matrix

The test setup, described in Derveni et al. [21], is composed of two CFS studs and two sheathing panels connected with each other by a system of in total eight fasteners (two fasteners per flange). Fig. 1 illustrates the test specimen configuration attached to the test rig via steel plates at top and bottom of the stud webs. Steel plates installed on the interior side of the webs restrain the webs from local deformation and provide fixity to the studs. Dimensions and cross-sections of the components used to construct the CFS-to-sheathing connection specimens are presented in Table 1. The test rig and setup is influenced by Winter (Green et al. [30], Winter [31]) and it is widely used and modified by different relevant connection testing efforts (Vieira and Schafer [27], Peterman et al. [25], Derveni et al. [21]) from which the current testing assumptions are adopted.

Two sheathing types were selected for this experimental study. The first type is a typical 19.05 mm (0.75 in.) thick fiber cement board (FCB) and the second type is a typical 16.59 mm (0.65 in.) thick steel-gypsum (SG) composite panel at which a 0.719 mm (0.0283 in.) thick light-gauge steel ply on the interior is adhered to a 15.875 mm (5/8 in.) thick gypsum panel on the exterior.

For the FCB panel specimens, two different screw types of the same diameter but of a different shank length, thread location and length, and drill bit are tested. The two fasteners represent available off-the-shelf options for fiber cement board attachment. The first type is an M4 × 50 (No. 8) self-drilling screw provided from the manufacturer and it is denoted in this work as screw "a", while the second type is a common M4 × 40 (No. 8) self-drilling screw denoted as screw "b". For the SG composite panel case, the common screw type "b" (M4 × 40 (No. 8)) is used in the testing.

Two fastener spacings are selected for the CFS-to-SG connection specimens: 152.4 mm (6 in.) and 304.8 mm (12 in.). For the CFS-to-FCB connection specimens, a 304.8 mm (12 in.) spacing is maintained due to the little response variability that results from the two different spacings. Screw edge distance from the sheathing is 38.1 mm (1.5 in.) as required by AISI-S100-16 [32].

The test matrix is shown in Table 2. Nine of the 18 experimental specimens are subjected to monotonic loading and the remaining nine specimens are subjected to cyclic loading. Three repetitions are conducted for every sheathing-screw configuration (as in Tao et al. [26]), to capture variability in response.

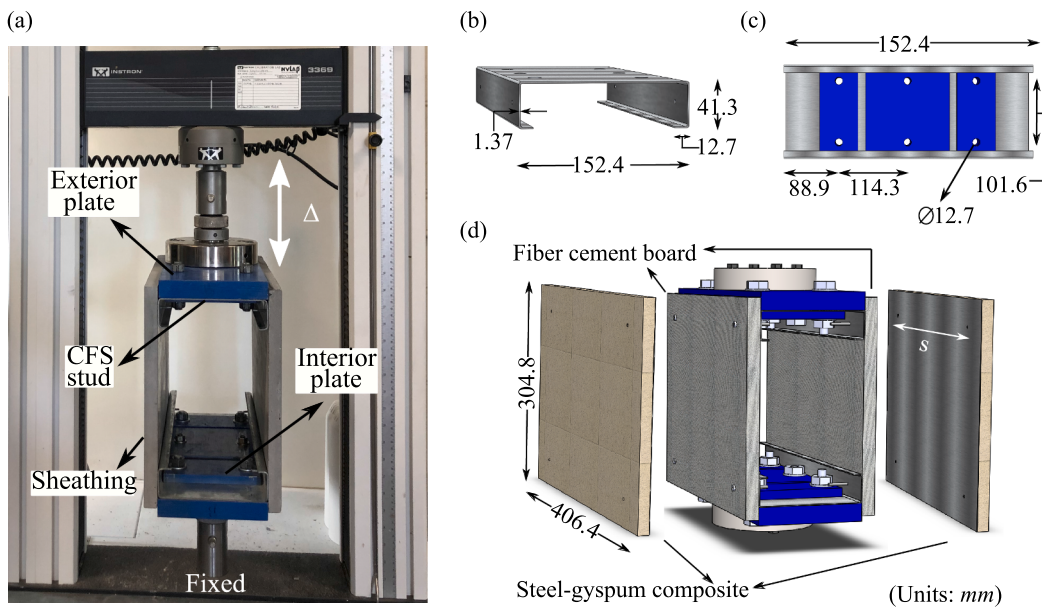


Fig. 1. CFS-to-sheathing connection experimental setup. (a) Photo of the actual specimen and test rig, (b) Cross-sectional stud dimensions, (c) Inside view of the specimen illustrating web restraint, and (d) isometric view of specimen and rig (fiber cement board or steel-gypsum composite board is used as sheathing material).

Table 1

Experimental specimen components, dimensions and details for the sheathing-screw test configurations. Three different configurations are tested by selecting different sheathing-screw assemblies.

Component	Cross-sectional dimensions (mm)
CFS Studs	152.4 web, 41.3 flange, 12.7 lip, 1.37 thickness
FCB Sheathing	304.8 length, 406.4 width, 19.05 thickness
SG Sheathing	304.8 length, 406.4 width, 16.59 thickness *
Exterior plates	406.4 length, 152.4 width, 25.4 thickness
Interior middle plates	139.7 length, 139.7 width, 12.7 thickness
Interior corner plates	63.5 length, 139.7 width, 12.7 thickness
Self-drilling screw "a"	M4 × 50, flat head
Self-drilling screw "b"	M4 × 40, flat head

* Composite: 0.719 mm thick steel adhered to 15.875 mm thick gypsum

2.2. Monotonic testing

Monotonic loading is applied at the top of the CFS-to-sheathing specimens via displacement control. Specifically, the specimens are subjected to tension at the top, while the bottom part is fixed (Fig. 1). A rate of 0.028 mm/s (0.0011 in./s) was used during the experiments and a pre-test seating load of 45 kN (10 lbs) was applied prior to each test. The monotonic tests were conducted before the cyclic tests to obtain the reference displacements required to construct the cyclic protocol.

2.3. Cyclic testing

The CUREE protocol derived by Krawinkler et al. [33] was used for cyclic testing. This protocol has been used in relevant CFS connection experimental programs (Peterman et al. [25], Okasha [34], Fiorino et al. [35], Fiorino et al. [36]), and shear wall programs (Liu et al. [4], Branston et al. [3], DaBreo et al. [6], Hoehler et al. [14]) and is adopted herein. The protocol is defined by a reference displacement (Δ) equal to 60% of the displacement at 80% of the monotonic post-peak load (Δ_m). The CUREE protocol is constructed of initiation, primary and trailing cycles as shown in Fig. 2. Each cycle was applied over 16 s (frequency equal to 0.0625 Hz). Fig. 2 also depicts the reference displacements determined from the monotonic tests.

Table 2

Test matrix of 18 stud-screw-sheathing specimens.

Loading	Sheathing Type	Screw Type	Repetition No.	Screw spacing (mm)
Monotonic	Fiber Cement Board	a	R ₁	304.8
			R ₂	304.8
			R ₃	304.8
	b	R ₁	304.8	304.8
			R ₂	304.8
			R ₃	304.8
Cyclic	Steel-Gypsum	b	R ₁	304.8
			R ₂	152.4
			R ₃	279.4
	Fiber Cement Board	a	R ₁	304.8
			R ₂	304.8
			R ₃	304.8
	b	R ₁	304.8	304.8
			R ₂	304.8
			R ₃	304.8
	Steel-Gypsum	b	R ₁	152.4
			R ₂	304.8
			R ₃	152.4

2.4. Test results

The force-displacement responses of 18 tests are depicted in Fig. 3. The resultant peak strength (P_{max}), initial stiffness (K_{in} : 0–40% peak load) and secant stiffness (K_{sec} : 0–100% peak load) of all tested connection specimens are included in Table 3 and Table 4 for monotonic and cyclic tests, respectively.

For monotonic tests, strength, stiffness and failure modes are varied between the different examined configurations. FCB specimens fastened with screw "a" exhibited little variability. Screw pull-through accompanied by sheathing tear out governed response, and was initiated by screw tilting. Shear screw failure occurred in some of the screws post-peak. FCB specimens fastened with screw "b" exhibited variability in one test, likely due to an over-driven fastener. Screw shear failure and

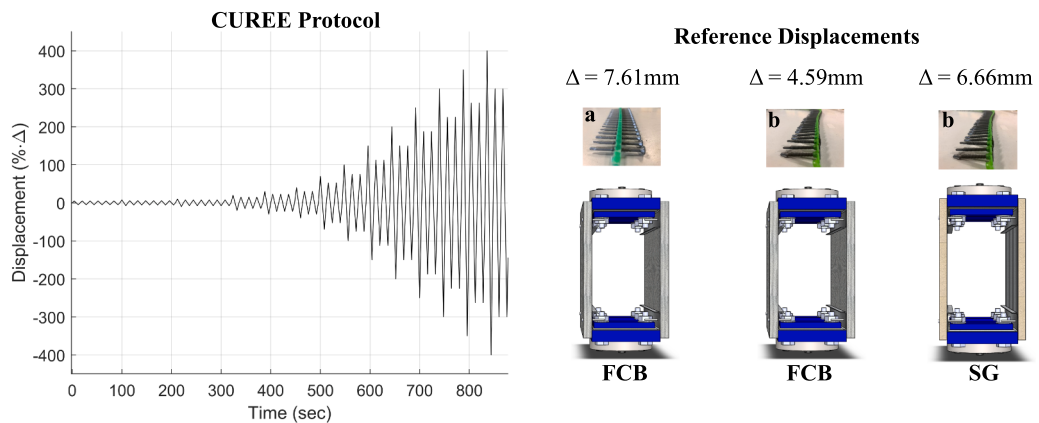


Fig. 2. Resultant cyclic protocol (time vs. displacement as a % of reference displacement) and reference displacements from each specimen type used to scale the protocol.

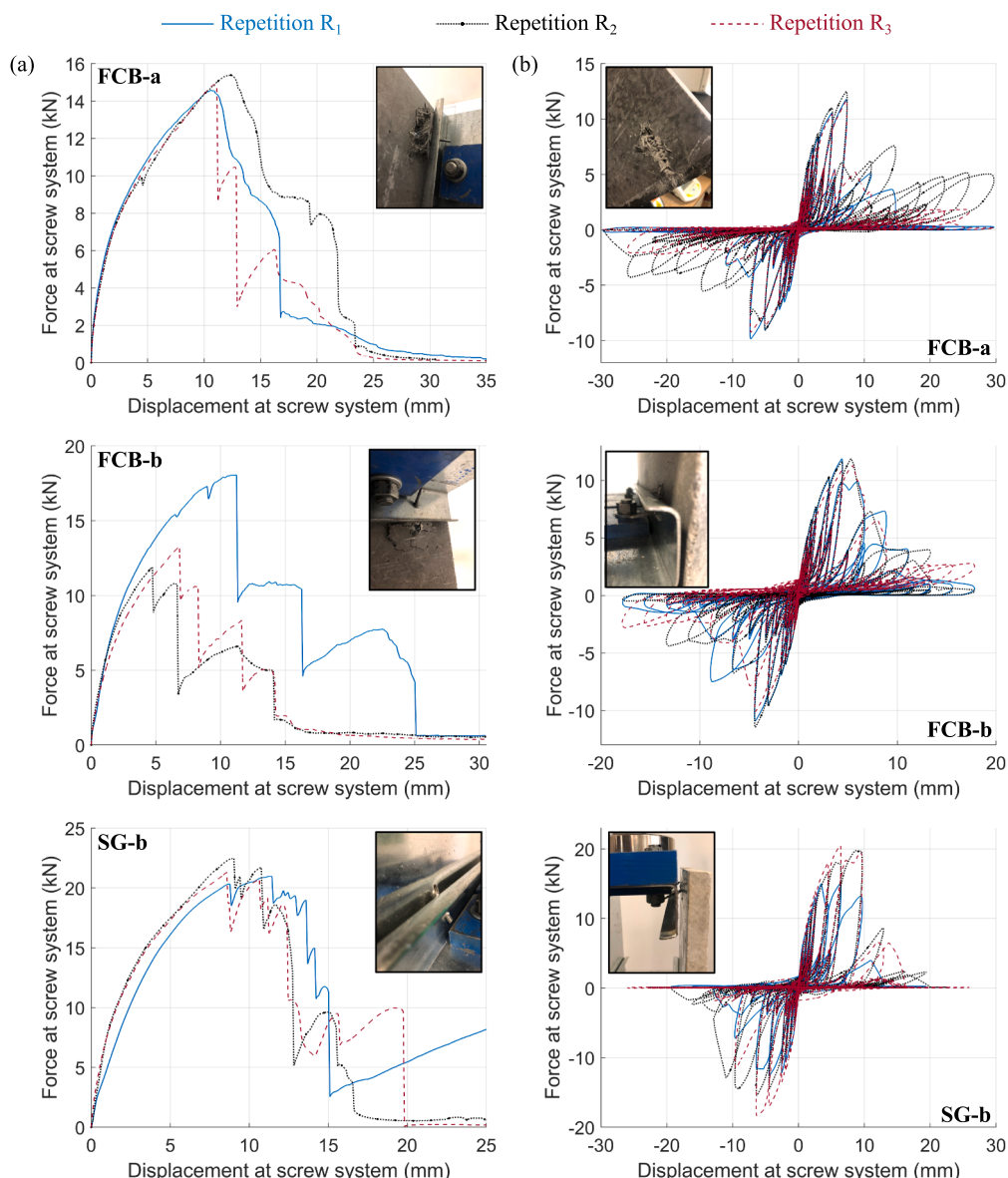


Fig. 3. Experimental force–displacement system response of 18 connection tests: (a) monotonic results, and (b) cyclic tests. Inset photographs demonstrate dominant failure mechanism.

Table 3

System test results of the nine monotonic experiments of CFS-to-sheathing shear connections. Peak load (P_{max}), initial stiffness (K_{in}) and secant stiffness (K_s) are shown for each sheathing-screw configuration (FCB-a, FCB-b, SG-b) and each test repetition (R_1 , R_2 , R_3).

Monotonic Connection Testing			
Test assembly	Peak strength	Initial stiffness	Secant stiffness
	P_{max} (kN)	K_{in} (kN/mm)	K_s (kN/mm)
FCB - a - R_1	14.579	4.596	1.372
FCB - a - R_2	15.383	4.005	1.243
FCB - a - R_3	14.883	4.142	1.366
FCB - b - R_1	18.051	4.749	1.608
FCB - b - R_2	11.920	5.277	2.521
FCB - b - R_3	13.285	4.424	1.947
SG - b - R_1	20.992	4.390	1.846
SG - b - R_2	22.485	6.989	2.491
SG - b - R_3	21.308	7.008	2.485

Table 4

System test results of the nine cyclic experiments of CFS-to-sheathing shear connections. Peak load (P_{max}), initial stiffness (K_{in}) and secant stiffness (K_{sec}) are shown for each sheathing-screw configuration (FCB-a, FCB-b, SG-b) and each test repetition (R_1 , R_2 , R_3). The + refers to results in positive quadrant and - to the results in negative quadrant.

Cyclic Connection Testing						
Test assembly	Peak strength		Initial stiffness		Secant stiffness	
	P_{max}^+ (kN)	P_{max}^- (kN)	K_{in}^+ (kN/mm)	K_{in}^- (kN/mm)	K_{sec}^+ (kN/mm)	K_{sec}^- (kN/mm)
FCB - a - R_1	12.369	- 10.318	4.442	4.700	1.625	1.354
FCB - a - R_2	13.090	- 9.5116	4.601	3.787	1.719	1.783
FCB - a - R_3	12.356	- 9.7672	4.188	4.637	1.622	1.282
FCB - b - R_1	12.428	- 11.438	5.966	5.630	2.702	2.488
FCB - b - R_2	12.691	- 12.022	6.045	5.429	2.219	2.614
FCB - b - R_3	11.825	- 10.584	5.546	5.341	2.019	2.301
SG - b - R_1	15.772	- 13.190	10.22	9.674	2.368	2.826
SG - b - R_2	20.945	- 16.248	6.462	5.951	2.279	2.436
SG - b - R_3	21.353	- 19.104	7.900	8.335	3.201	2.865

sheathing tear out dominated response. Similarly, the failure was initiated by screw tilting eventually leading to shear failure post peak, accompanied by bearing and edge tear out.

In steel-gypsum composite board specimens, force-displacement results demonstrated low variability. Shear screw failure was the governing failure mechanism. At the beginning of the tests, screw tilting was observed, which was followed by the shear failure of the screws and sheathing bearing (both steel and gypsum) around the screw location. The steel and gypsum separate in the post-peak regime in two tests.

Cyclic strength and stiffness were similar to those determined in monotonic testing for the various tested configurations. In general, cyclic tests demonstrated lower strength and higher stiffness in comparison to monotonic tests, as shown in Section 3. FCB specimens fastened with screw "a" exhibited little variability in strength and stiffness. One of the tests (second repetition) slightly differed in the energy dissipation post-peak, since higher energy dissipation capacity was observed at larger drifts compared to the rest of the specimens. The response of the specimens was governed by shear screw failure followed by FCB sheathing bearing around screw locations and/or sheathing edge tear out.

FCB specimens fastened with screw "b" displayed consistent behavior in terms of strength, stiffness and energy dissipation. Shear screw failure accompanied by sheathing bearing at the locations of the screws

governed the behavior of these connections within the repetitions. Energy dissipation capacity was lower compared to FCB-specimens fastened with screw "a".

In steel-gypsum composite board specimens, shear connection behavior demonstrated strength variability in one test (first repetition), likely because of an over-driven screw. The governing failure mechanisms were shear screw failure and localized bearing of the SG composite material around the screws. Edge separation between steel and gypsum of the composite sheathing panel may have been present towards the end of the tests post peak. Fastener spacing did not impact strength, stiffness and energy dissipation of the specimens.

Connection ductility is implicit to screw type and the different failure mechanisms. For monotonic tests, when pull-through dominates fastener response, higher ductility is observed in the connection specimens (FCB-a) in comparison to shear screw failure driven specimens (FCB-b and SG-b) which demonstrate abrupt capacity drops post-peak. For cyclic tests, higher ductility is also shown in FCB-a specimens in comparison to FCB-b and SG-b specimens.

3. Backbones and hysteretic parameters of CFS-to-FCB and CFS-to-SG connections

The eight-fastener system response is converted into single screw response by using the equations (Eq. (1); Eq. (2); Eq. (3)) derived by Vieira and Schafer [27]. If P is the eight-fastener system load, Δ is the eight-fastener system displacement, and K is the eight-fastener system stiffness:

$$P_i = P/4. \quad (1)$$

$$\Delta_i = \Delta/2. \quad (2)$$

$$K_i = K/2. \quad (3)$$

where the subscript i denotes individual fastener parameters. Once results are converted to individual fastener values, cyclic backbones are determined to calculate hysteretic parameters for a Pinching4 characterization. This characterization is provided herein as a tool for future reduced-order computational modeling efforts.

3.1. Monotonic testing

The average fit to data of the monotonic experiments are taken at 40% of the peak load, 80% of the peak load, 100% of the peak load and 30% post-peak load (Derveni et al. [21]). The behavior of each different sheathing-screw assembly (FCB-a, FCB-b, SG-b) is obtained by averaging the three test repetitions (R_1 , R_2 , R_3) of each of the assemblies, as illustrated in Fig. 4 (left graphs). The average fit to data parameters are summarized in Table 5. Table 6 contains the average stiffness calculations of the different regions within the four-point mean response.

Determining the average experimental response enables quantitative comparison between specimen configurations, with the impact of variability reduced due to averaging. The strength between the two types of screws of the CFS-to-FCB connection specimens does not significantly differ; the average strength of FCB-a is higher than FCB-b by a percentage of 3.66%. The initial stiffness for screw "b" specimens is higher than that of screw "a" specimens, by 13%. CFS-to-SG connections result to higher strength capacity in comparison with the CFS-to-FCB specimens. In particular, SG-b assembly average strength is higher than FCB-a strength by 45% and higher than FCB-b strength by 50%. SG-b average initial stiffness is higher by 39% in comparison to FCB-a specimens and by 23% in comparison to FCB-b specimens.

3.2. Cyclic testing

Pinching4 parameters are extracted from cyclic test hystereses. Pinching4 is a uniaxial model initially developed by Lowes et al. [37] and Altoontash [38] to characterize cyclic load-displacement response

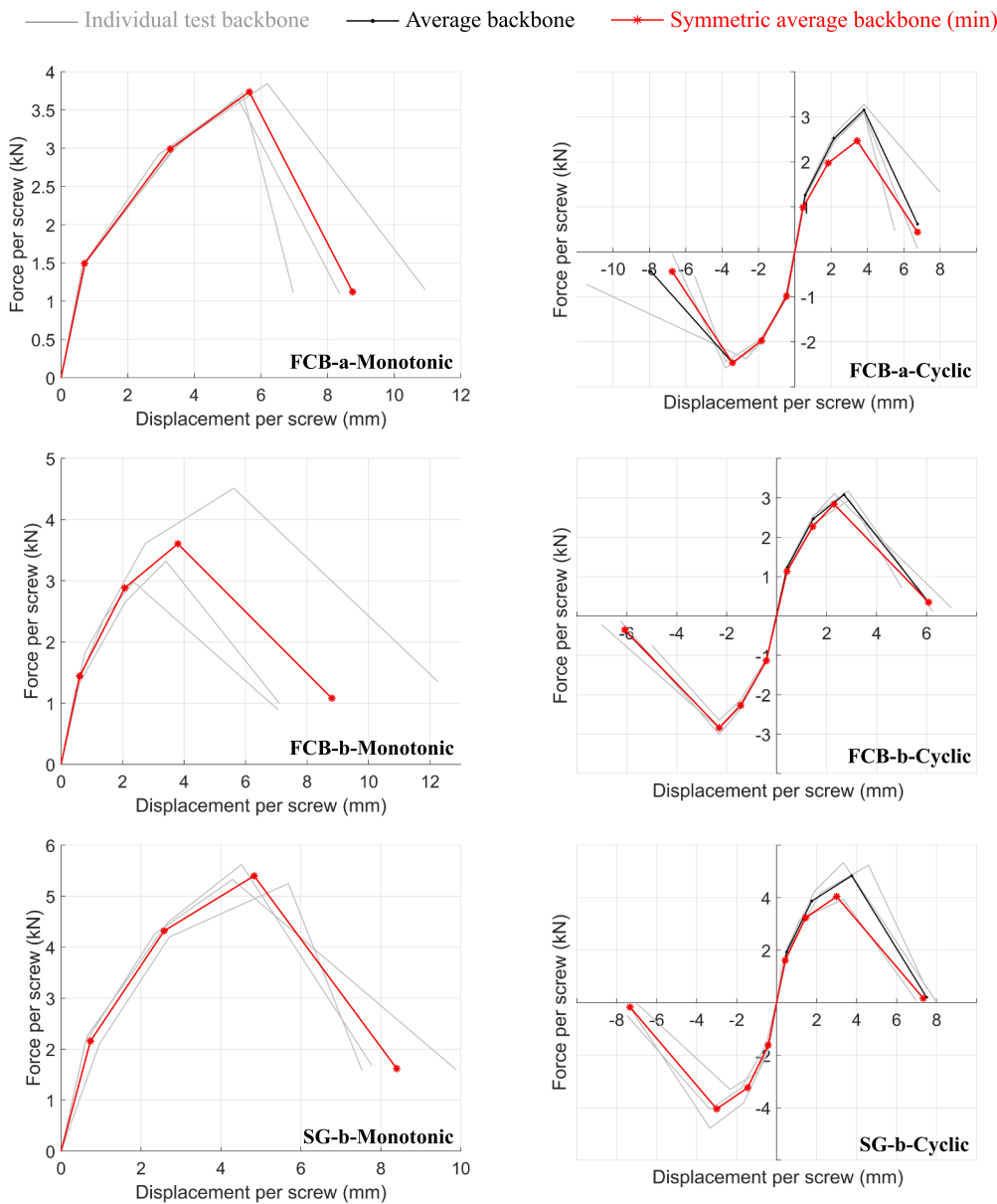


Fig. 4. Average backbone parameters for both monotonic (left graphs) and cyclic (right graphs) loading.

parameters for re-loading and un-loading in reinforced concrete, which can exhibit a severely pinched hysteretic response when damaged. This severe pinching is also exhibited in CFS connections, and as a result the Pinching4 model has seen wide adoption by the CFS research community (Peterman et al. [25], Tao et al. [26], Buonopane et al. [17], Liu et al. [4]). Pinching4 parameters are defined in Fig. 5. Points A-H in Fig. 5 represent the backbones of the tests, while points a-f represent the hysteretic parameters. Symmetry in the positive and negative quadrants is enforced.

The displacement at the fourth point of each quadrant (D and H) are selected at lower drift points in order to avoid ductility and energy overprediction and to provide realistic connection behavior. Experimental responses are averaged, and the minimum of the positive and negative quadrant response is chosen for symmetry. Table 5 summarizes the backbone parameters and Table 6 the stiffness values.

The un-loading ($uForceP$, $uForceN$) and re-loading parameters ($rDispP$, $rForceP$, $rDispN$, $rForceN$) of the Pinching4 model are calculated based on the squared error minimization of the cumulative energy between the test and the Pinching4 model, as well as the error

minimization of energy at each cycle. This optimization method is implemented in MATLAB [39]. Comparisons of the cumulative energy of the Pinching4 model in comparison to the experiments are illustrated in Fig. 6 for all tested configurations. The un-loading parameters $uForceP$ and $uForceN$ are maintained constant and equal to 0.001 during the optimization process, based on Peterman et al. [25]. Average hysteretic parameters are obtained for each sheathing-screw configuration for the first and third quadrant. Symmetric parameters are finally proposed by averaging the positive and the negative response, as depicted in Table 5. The Pinching4 characterizations compared to the experimental results are shown in Fig. 7.

Average cyclic test response results to lower strength and higher stiffness in comparison to the respective monotonic testing average response. Shear capacity of FCB-b cyclic specimens is higher by 15% and initial stiffness is higher by 26% in comparison to FCB-a specimen cyclic response. Across testing, SG specimens were stronger than FCB specimens by 42–64%. Similarly, SG specimens were stiffer than FCB counterparts, through fastener type on FCB specimens accounted for larger variation, between 39% and 75%.

Table 5

Monotonic backbone CFS-to-sheathing connection shear behavior and cyclic Pinching4 connection characterization. The proposed parameters are based on a three-test average of each sheathing-screw configuration (FCB-a, FCB-b, SG-b). Symmetric positive and negative parameters are introduced.

Monotonic Connection Testing								
Type	Backbone parameters (mean) *							
	ePd ₁ (mm)	ePd ₂ (mm)	ePd ₃ (mm)	ePd ₄ (mm)	ePf ₁ (kN)	ePf ₂ (kN)	ePf ₃ (kN)	ePf ₄ (kN)
FCB - a	0.707	3.275	5.650	8.753	1.495	2.990	3.737	1.121
FCB - b	0.604	2.074	3.797	8.803	1.442	2.884	3.605	1.081
SG - b	0.736	2.579	4.829	8.395	2.160	4.319	5.399	1.620

Cyclic Connection Testing								
Type	Pinching4 backbone parameters (mean) *							
	ePd ₁ (mm)	ePd ₂ (mm)	ePd ₃ (mm)	ePd ₄ (mm)	ePf ₁ (kN)	ePf ₂ (kN)	ePf ₃ (kN)	ePf ₄ (kN)
FCB - a	0.454	1.838	3.429	6.750	0.987	1.973	2.466	0.437
FCB - b	0.415	1.447	2.299	6.083	1.135	2.270	2.837	0.348
SG - b	0.426	1.449	3.001	7.333	1.618	3.236	4.045	0.169

Type	Pinching4 un- and re-loading parameters (mean) *		
	rDispP	rForceP	uForceP
FCB - a	0.437	0.027	0.001
FCB - b	0.346	0.046	0.001
SG - b	0.412	0.017	0.001

* Symmetric negative parameters

4. Computational analysis of FCB- and SG-sheathed CFS shear walls

The fundamental finite element modeling assumptions are adopted from Derveni et al. [21], in which the introduced modeling approach is validated by various experimental studies for OSB-sheathed CFS shear wall systems and by a complete parametric analysis of the modeling assumptions. Derveni et al. [21] concludes that fastener-based CFS shear wall modeling is able to capture strength, stiffness and wall failure modes and highlights that CFS-to-sheathing shear connection response is the main parameter that affects the overall wall capacity. The current work expands the abilities of fastener-based modeling methods towards the FCB- and SG-sheathed CFS shear walls.

The finite element response of each shear wall is obtained via a two-stage approach, including an initial linear elastic analysis followed by the final pushover analysis. A two-stage approach is necessary as CFS-to-sheathing vector forces are misaligned with the global coordinate system axes after loading has begun. A local coordinate system is introduced at each fastener characterized by the angles obtained from prior linear elastic analyses. In stage A, a linear elastic analysis is performed to determine vector directions. Material plasticity, geometric nonlinearities and connection nonlinearities are eliminated to obtain the vector directions. In stage B, the local coordinate systems from the fastener force vectors are introduced, and a pushover analysis is conducted. The two-stage approach reduces and nearly eliminates overestimation of connection capacities, as will be demonstrated in the discussion of the results.

4.1. Model description and geometry

The archetypal shear wall configuration adopted for the modeling program is 1.22 m × 2.44 m (4 ft × 8 ft), with a 2:1 aspect ratio, as required by AISI-S400 [1]. The structural archetype is illustrated in

Table 6

Monotonic and cyclic stiffness calculation for CFS-to-sheathing connections at the four-point backbone average curves. K_1 , K_2 , K_3 , K_4 represent the stiffness between 0–40% peak load, 40–80% peak load, 80–100% peak load, 100%-last point post peak load, respectively.

Sheathing screw	K_1 (kN/mm)	K_2 (kN/mm)	K_3 (kN/mm)	K_4 (kN/mm)
Monotonic Connection Testing				
FCB - a	2.115	0.582	0.315	– 0.843
FCB - b	2.387	0.981	0.418	– 0.504
SG - b	2.935	1.171	0.480	– 1.060
Cyclic Connection Testing				
FCB - a	2.174	0.712	0.310	– 0.611
FCB - b	2.735	1.100	0.665	– 0.658
SG - b	3.798	1.582	0.521	– 0.895

Fig. 8. The CFS frame is composed of back-to-back chord studs, a field stud and top and bottom tracks. FCB or SG sheathing is attached on the exterior side of the structural frame and hold-downs are used at the bottom part of the wall to resist the overturning moment. Aligned with AISI-S400, four common fastener patterns are included in the modeling suite: 152.4 mm (6 in.), 101.6 mm (4 in.), 76.2 mm (3 in.), and 50.8 mm (2 in.). Fasteners along the perimeter are installed 12.7 mm (1/2 in.) from the sheathing edges. The fastener spacing in the field to the wall was set as 304.8 mm (12 in.). CFS stud and track cross-sections, FCB and SG sheathing thicknesses, and CFS-to-sheathing connection screw types are described in Table 1 and Fig. 8. Simpson Strong-Tie S/HD10S hold-downs are used at the bottom of the wall configuration. The selected wall configuration is based on the experimental setup of McGill University (Branston [40] - numerically validated by Derveni et al. [21]) by altering the sheathing material and thickness (from OSB to FCB and SG) and the CFS thickness to accurately approach the purpose of this study using the experimental connection data extracted in the previous section.

4.2. Element type and mesh size

CFS components and FCB and SG sheathing components are modeled with shell elements. Within the ABAQUS element library, S4R elements were selected, representing general purpose four-sided elements with linear shape functions and reduced integration to avoid shear locking. A mesh size of 6.35 mm (0.25 in.) was chosen for the CFS members and a coarser mesh of 50.8 mm (2 in.) was selected for FCB and SG sheathing (Derveni et al. [21]). The mesh is illustrated in Fig. 9.

4.3. Material properties

CFS components are modeled as isotropic and elastic perfectly-plastic. The modulus of elasticity is 203 GPa (29500 ksi), the yield strength is 345 MPa (50 ksi) and the Poisson's ratio is equal to 0.3.

As fastener failures dominate response, the FCB sheathing is simulated as elastic isotropic material with a modulus of elasticity of 8963 MPa (1300 ksi), as provided from the manufacturer.

The SG composite sheathing is modeled as elastic isotropic material through a composite section definition in ABAQUS, which allows for plies with different moduli of elasticity. The light gauge steel ply is simulated by using a modulus of elasticity of 203 GPa (29500 ksi) and the gypsum ply is modeled by using modulus of elasticity of 3479 MPa (505 ksi) (Gypsum Association [41]). The gypsum bending stiffness (EI_g) is given as 440–1160 kN-mm²/mm (3000–8000 lb-in.²/in.) and it is converted to Young's modulus (1320–3479 MPa) through Eq. (4) (upper bound is used herein).

If $(EI)_g$ is the gypsum bending stiffness and t_g is the gypsum thickness, the gypsum Young's modulus is defined as:

$$E_g = 12(EI)_g/t_g^3 \quad (4)$$

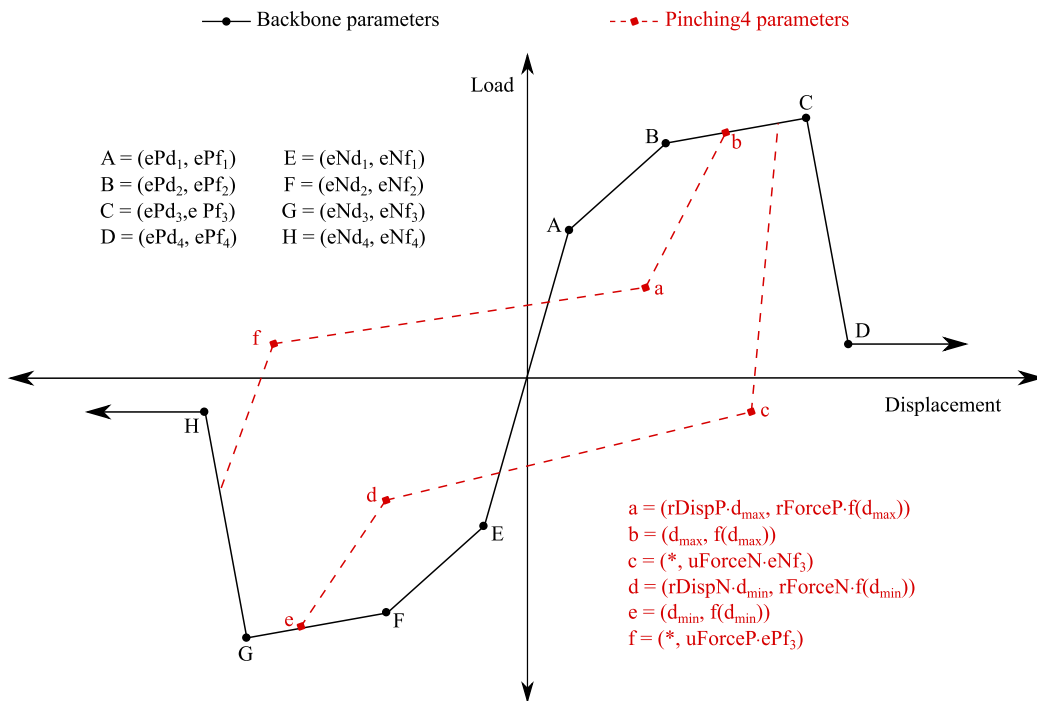


Fig. 5. Pinching4 uniaxial model parameters. Four-point backbones and un-loading and re-loading parameters (hysteretic parameters) are denoted by uppercase letters and lowercase letters, respectively.

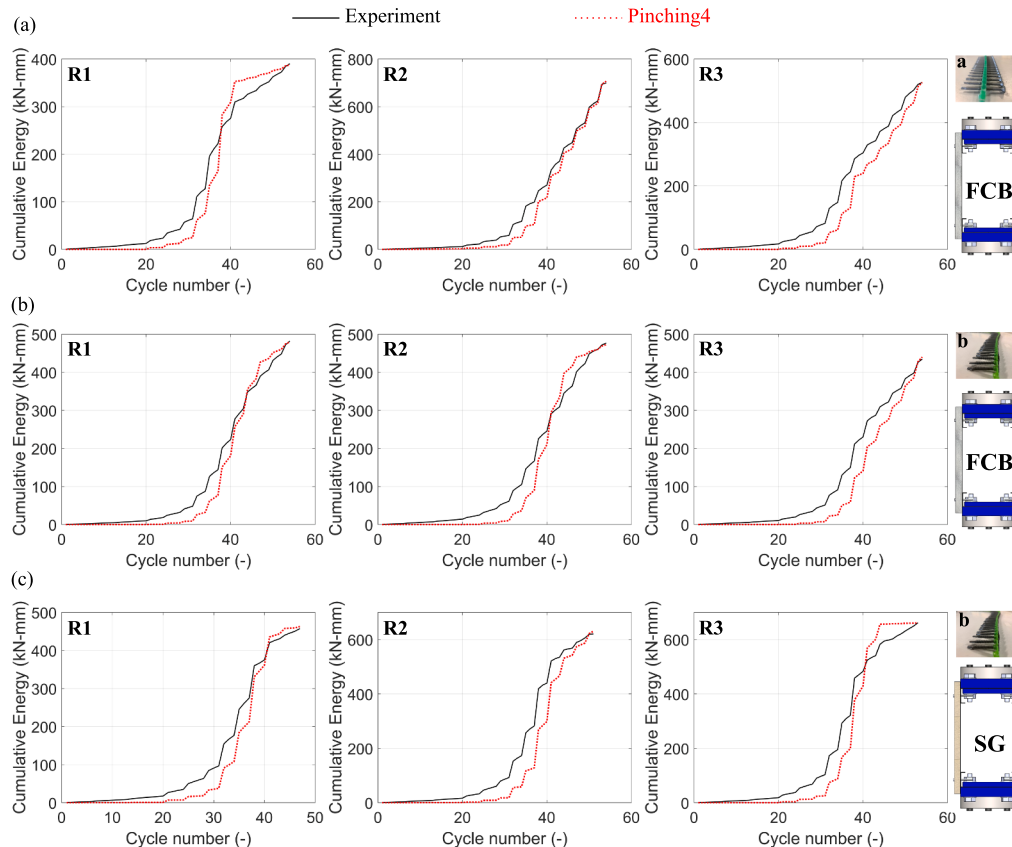


Fig. 6. Cumulative energy comparison between Pinching4 model and the respective experimental results for single fasteners. (a) CFS-to-FCB screw type a, (b) CFS-to-FCB screw type b, and (c) CFS-to-SG screw type b.

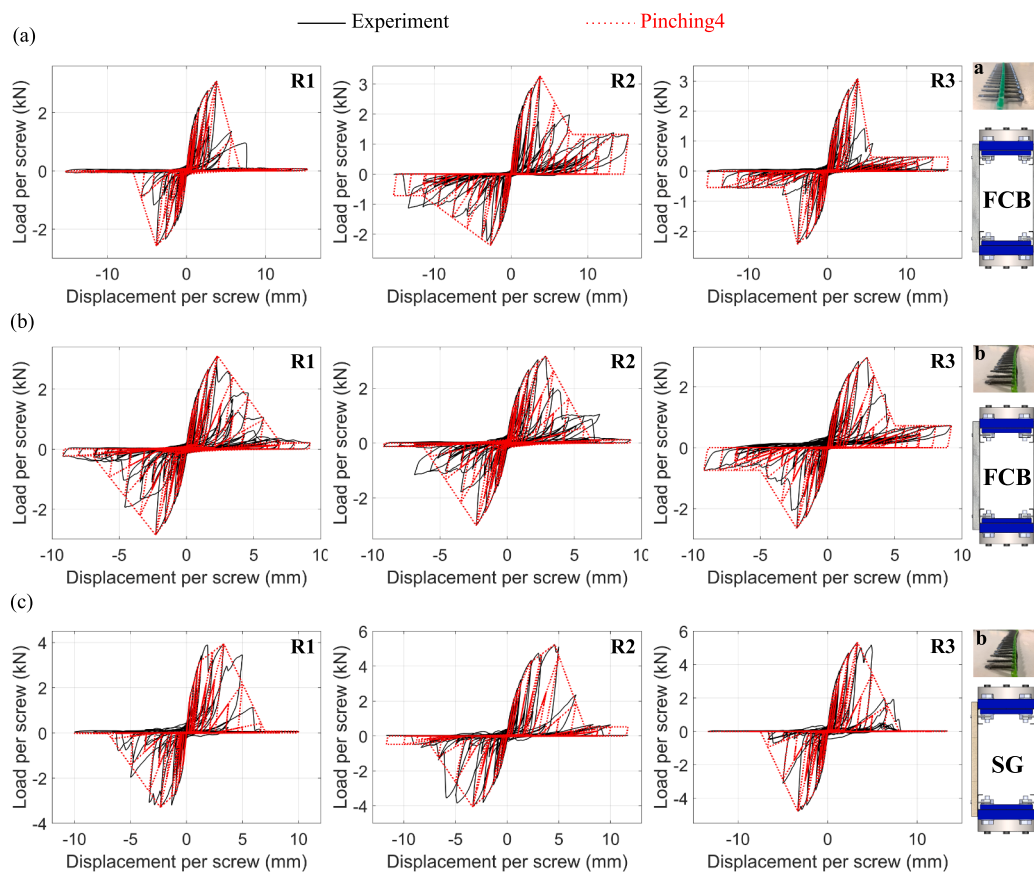


Fig. 7. Pinching4 response in comparison with the respective experimental results for single fasteners. (a) CFS-to-FCB screw type a, (b) CFS-to-FCB screw type b, and (c) CFS-to-SG screw type b.

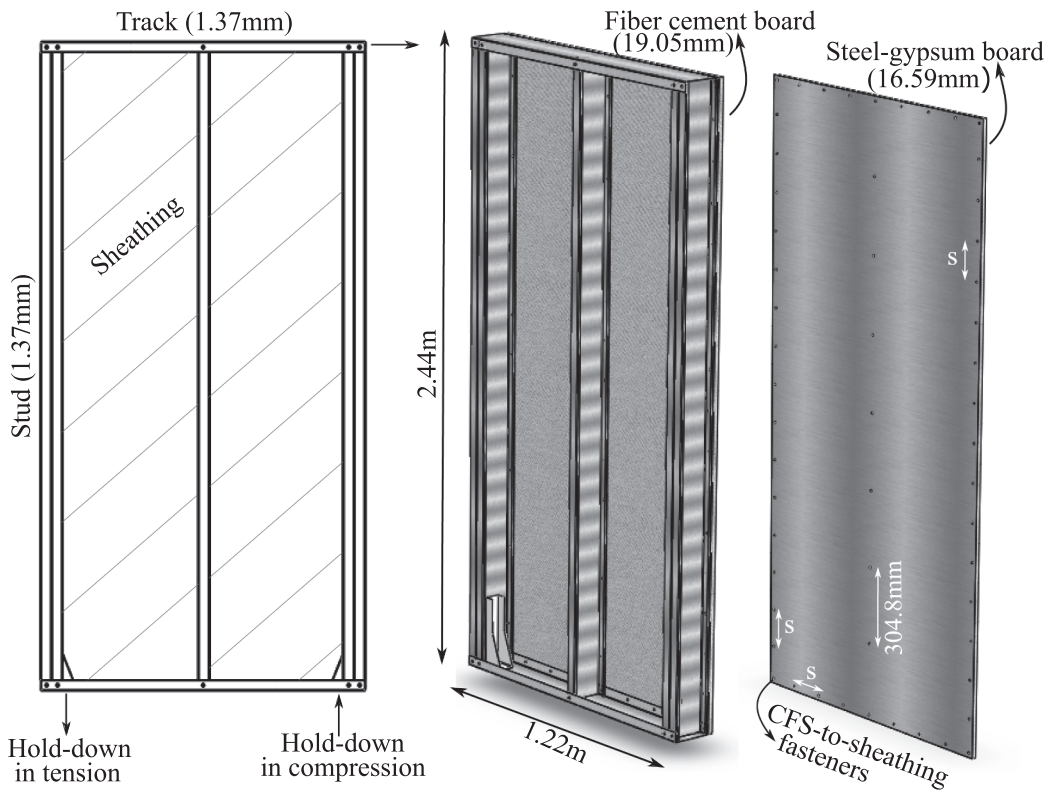
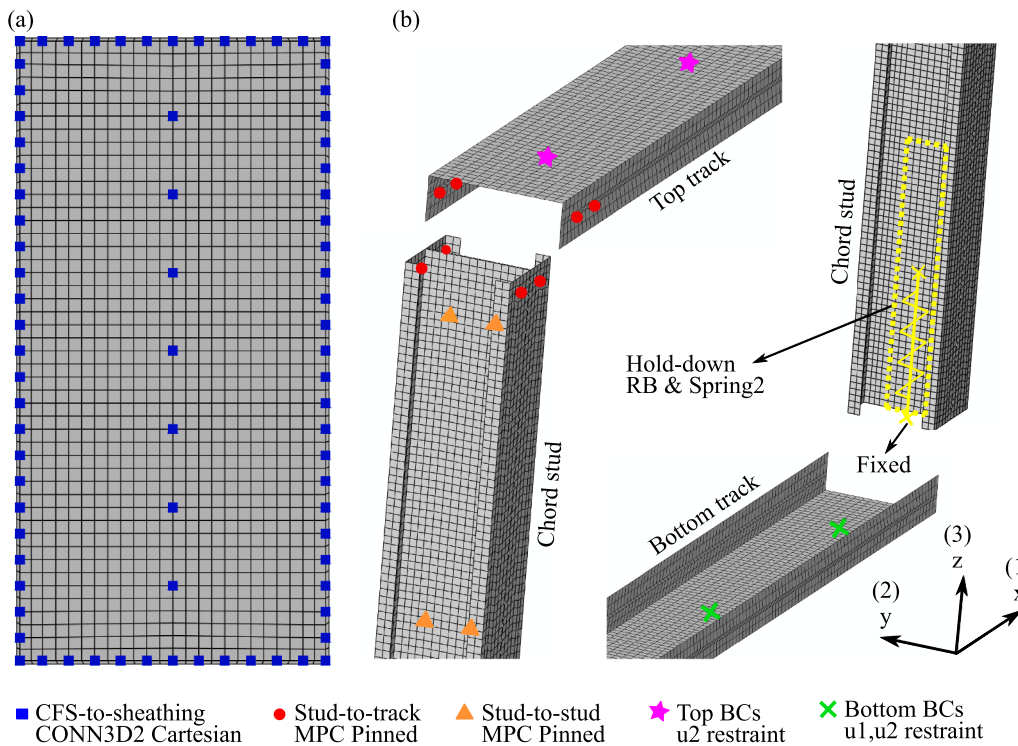


Fig. 8. CFS shear wall configuration used in finite element modeling (fiber cement board or steel-gypsum composite sheathing is attached; where s is the perimeter fastener spacing).



4.4. Connection simulation and interactions

Connection simulation is segregated by cold-formed steel to cold-formed steel (CFS-to-CFS) connections, and cold-formed steel to sheathing (either FCB or SG) connections.

CFS-to-CFS connections (stud-to-track and stud-to-stud) are modeled via multi-point pinned constraints (MPC pinned). This enforces equal displacements of the two nodes and leaves independent the rotations. The first selected node is the dependent node at which the degrees of freedom are eliminated, while the second selected node is the independent node. Fig. 9b illustrates the stud-to-track connections in the center of their flanges. Fig. 9b also depicts the two lines of connections between back-to-back chord studs spacing 304.8 mm (12 in.) vertically.

CFS-to-FCB connections and CFS-to-SG connections are modeled through nonlinear connector elements CONN3D2 Cartesian, as shown in Fig. 9a. These are two-node springlike elements with local coordinate systems at which independent behavior is allowed for the three translational degrees of freedom. The first selected node is located on the sheathing, while the second and dependent to the first node is chosen on the CFS component flanges. For the two shear local directions, the experimentally-obtained behavior as determined in the previous experimental section is introduced in the model (monotonic data in Table 5) for all CFS-to-sheathing connections. Rigid elastic behavior ($k = 1750000 \text{ kN/m}$ (10000 kips/in.)) is assumed for the pull-out direction, to avoid sheathing out-of-plane movement. This assumption is consistent with experimental observations.

Contact definition is also introduced through contact pairs, in order to eliminate the out-of-plane penetration of the sheathing into the CFS structural frame. Hard contact is used with the FCB or SG sheathing as the master surface and the CFS track and stud flanges as the slave surfaces. Sheathing is selected as the master surface due to its relatively coarser mesh.

4.5. Boundary conditions and loading

At the top of the wall, the out-of-plane translation (direction 2 in

Fig. 9. FCB- and SG-sheathed CFS shear wall mesh and connection representation in ABAQUS software. (a) Sheathing mesh is illustrated and CFS-to-sheathing connections are indicated (CONN3D2 Cartesian), (b) Isometric exploded view of CFS components. CFS stud and track mesh size and connections between studs and tracks and between back-to-back studs are depicted (MPC pinned). Bottom track boundary conditions are illustrated and hold-down representation by a rigid body and a linear behavior through Spring2 (dashed lines) is shown.

Fig. 9b) of the wall is restrained by six nodes at the top of the track spacing 230 mm (9 in.), representing the attachment of the wall to the rig, based on Branston [40] experimental work (Fig. 9b).

At the bottom part of the wall, the track is restrained at four nodes representing the shear anchors that connect the wall to the foundation, as described by the Branston [40] experimental study. The horizontal and the out-of-plane translation (directions 1 and 2) of the wall are restrained (Fig. 9b).

Hold-downs are simulated by assuming rigid body behavior where they connect to the back-to-back chord studs. A reference point (RP) at the middle of each rigid body is connected to a fixed node in the foundation by a Spring2 element, as depicted in Fig. 9b. The Spring2 element is a two-node element which allows for introducing a behavior in a fixed degree of freedom; vertical displacement (direction 3) is restrained herein in order to prevent the uplift of the wall. Tensile stiffness is taken from manufacturer specifications (Simpson Strong-Tie Co. Inc. [42]) and is equal to 22292 kN/m (127.3 kips/in.). Compressive stiffness is equal to the tensile stiffness times a factor of 1000, as described by Leng et al. [43].

Loading is applied through displacement control at a reference point (RP) on the center of the top track. The cross-section of the top track is defined as a rigid body tied at the motion of the reference point. A monotonic displacement of 0.08 m (3.15 in.) is applied by using an initial and maximum time step of 0.01 and a minimum time step of 10^{-7} .

4.6. Finite element modeling results

The results for the three different configurations are shown in Fig. 10 for the four different fastener spacing patterns. The shear strength of the CFS-to-FCB shear walls between the two M4 (No. 8) types of screws, "a" and "b", varied little, approximately 0.02%–2.5%. Shear strength decreases as fastener spacing increases, by 25%–48% from 50.8 mm to 152.4 mm (2 in. to 6 in.). SG-sheathed shear walls have a higher shear capacity compared to FCB-sheathed shear walls, by 0.4%–45%, where capacity increase is highly dependent on fastener spacing. The impact of fastener spacing is discussed in the following paragraph. Initial stiffness increases 7%–20% in SG-sheathed shear walls

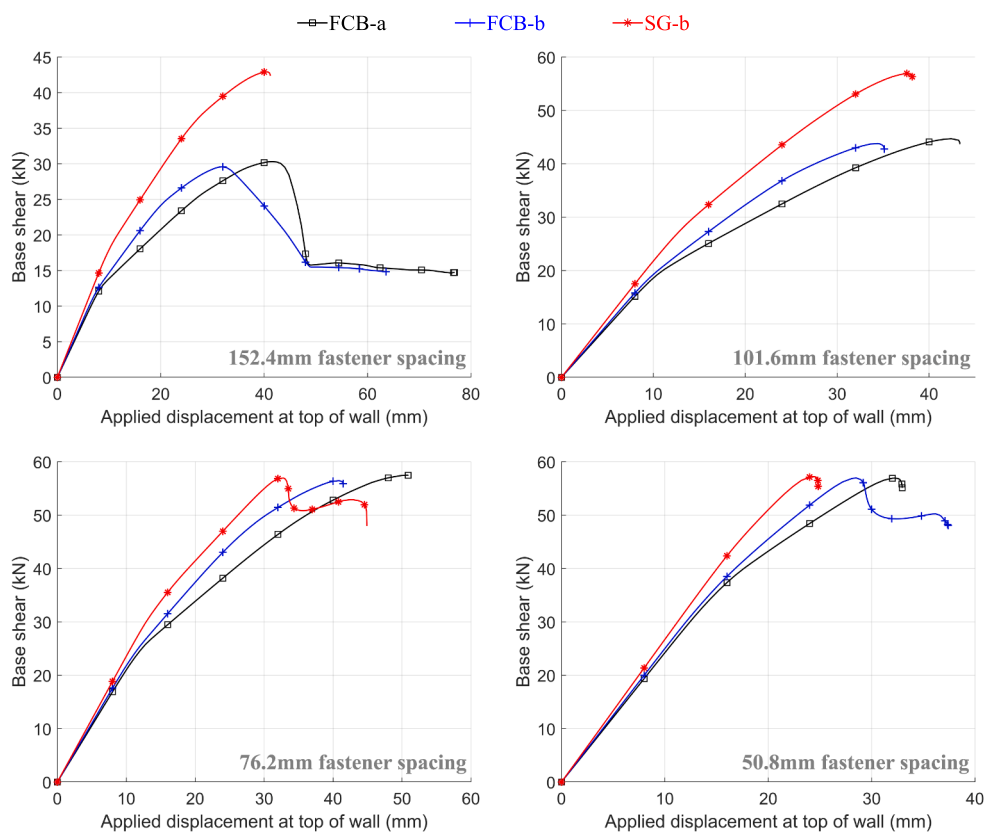


Fig. 10. Force–displacement response of CFS shear walls sheathed with FCB (screw a and screw b) and SG composite (screw b) for four different fastener spacing patterns (152.4 mm, 101.6 mm, 76.2 mm, 50.8 mm).

Table 7

Peak load (P_{max}), initial stiffness (K_{in} ; 0–40% peak load) and secant stiffness (K_{sec} ; 0–100% peak load) for the different CFS shear wall configurations and different fastener spacings.

Assembly type	Spacing (mm)	Peak strength	Initial stiffness	Secant stiffness
		P_{max} (kN)	K_{in} (kN/mm)	K_{sec} (kN/mm)
FCB - a	152.4	30.31	1.151	0.729
	101.6	44.71	1.874	1.054
	76.20	57.50	2.080	1.132
	50.80	56.95	2.422	1.768
FCB - b	152.4	29.58	1.604	0.924
	101.6	43.81	1.961	1.274
	76.20	56.45	2.172	1.384
	50.80	56.96	2.500	1.999
SG - b	152.4	42.92	1.808	1.073
	101.6	56.92	2.174	1.515
	76.20	56.96	2.325	1.737
	50.80	57.20	2.672	2.345

when compared to FCB-sheathed shear walls. Secant stiffness also increases in SG-sheathed shear walls in comparison to FCB-sheathed shear walls, by 16%–53%. Generally, walls fastened with screw “b” are stiffer than walls fastened with screw “a”, by 3%–6% and 13%–26% of initial and secant stiffness, respectively. Larger fastener spacings correspond to decreased initial and secant stiffness. Results are summarized in Table 7.

The perimeter fastener spacing impacts failure mechanisms in addition to strength and stiffness. For the 152.4 mm (6 in.) spacing, wall response is governed by CFS-to-sheathing fastener failures at the perimeter of the wall in all the examined configurations. Failure initiates of

the right bottom corner of each wall, propagates to all of the corners of the wall, and is then progressively distributed to the fasteners along the studs and tracks. This is true regardless of screw type or sheathing material. At 101.6 mm (4 in.) spacing, FCB-sheathed specimens are similarly governed by CFS-to-FCB connection failures, in which damage initiates and propagates as it did in the 152.4 mm (6 in.) case. In SG-sheathed specimens, however, the increased capacity and rigidity of the connections forces failure into the CFS framing, specifically the top track. The 76.2 mm (3 in.) spacing represents a bifurcation point for connection-dominant versus frame-dominant failure mechanisms. In FCB-sheathed specimens, both fastener failures and yielding of the top track occur. Once fastener spacing is further reduced to 50.8 mm (2 in.), failure is exclusively in the steel framing. At both 76.2 mm (3 in.) and 50.8 mm (2 in.) spacings, SG specimens failed via yielding of the top track.

Fastener spacing is thus a fundamental parameter in predicting the overall response of the wall, as failure mechanism is dependent on the fixity impacted to the sheathing by the fastener lines. Fig. 11 depicts the two-stage approach results and Fig. 12 illustrates these failure modes.

5. Shear capacity recommendations

The finite element modeling approach described herein is capable of providing predictions for base shear capacities per unit width (v_n). These are shown in Table 8. Similar to existing AISI-S400 [1] prescriptive methods for OSB-sheathed shear walls, Table 8 also accounts for sheathing thicknesses, CFS members thicknesses, fastener diameters and fastener spacings for the nominal capacity predictions. Since shear wall capacities herein are derived from a finite element model validated for OSB-sheathed walls, this work suggests future experimental efforts for FCB- and SG-sheathed walls. Based on the connection-level tests of this current study, FCB is expected to behave as a rigid body similar to OSB, and SG is expected to behave as a composite material (steel fully

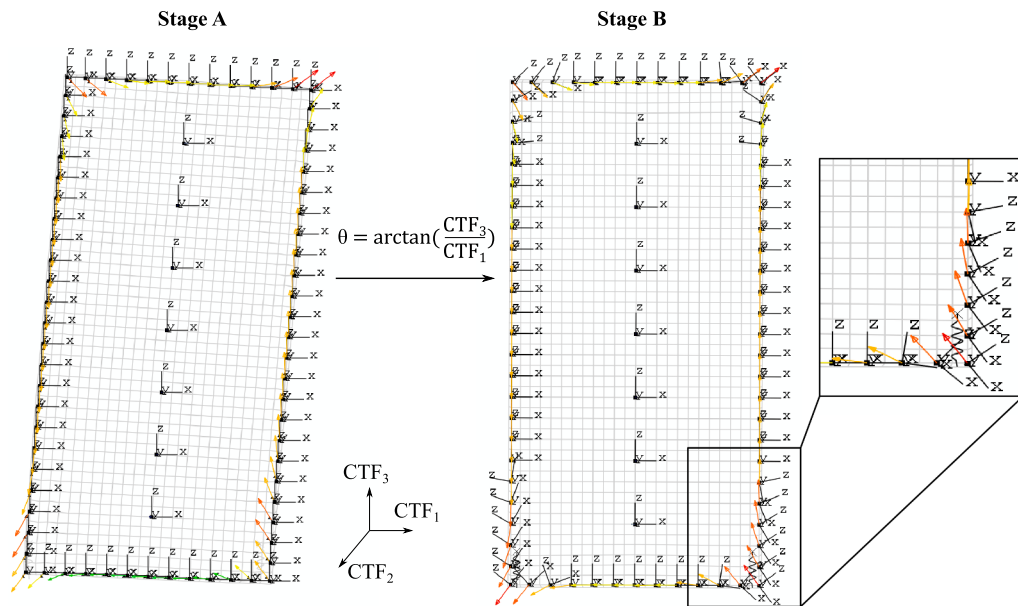


Fig. 11. Two-stage analysis procedure: at stage A, connection angles are calculated; at stage B these angles are used to define local coordinate systems for each connection.

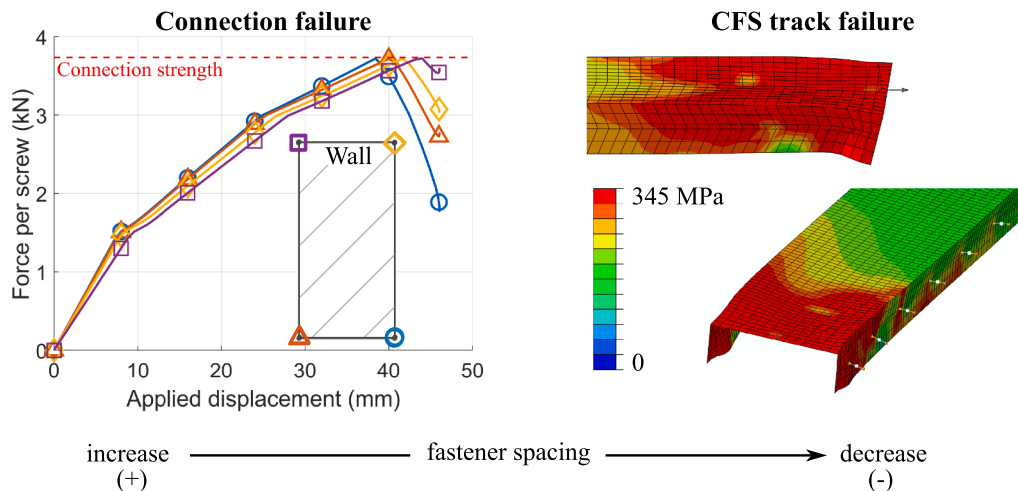


Fig. 12. Changing failure mode as fastener spacing decreases from CFS-to-sheathing connection failures to CFS framing (track) failures (von-Mises stress contours).

Table 8
Recommended design capacities for CFS shear walls sheathed with FCB and SG.

Assembly description	Aspect Ratio (<i>h</i> : <i>w</i>)	Shear per unit wall width (kN/m)				CFS Thickness (mm)	Screw Size		
		Screw Spacing (mm)							
		152.4	101.6	76.20	50.80				
19.05 mm FCB	2:1	24.86	36.67	47.16	46.71	1.37	M4a ¹		
19.05 mm FCB	2:1	24.26	35.93	46.30	46.72	1.37	M4b ²		
19.05 mm FCB	2:1	24.56	36.30	46.73	46.72	1.37	M4 ³		
16.59 mm SG	2:1	35.20	46.69	46.72	46.92	1.37	M4b ²		

1 Screw a type.

2 Screw b type.

3 Average of screw a and b.

adhered to gypsum) until peak load; though localized separation of steel and gypsum in the SG board due to partial failure of the adhesive connection may occur at peak or post-peak. However, existing experimental testing of SG-sheathed walls by Hoehler et al. [14] and Mohebbi et al. [9] indicate that failures are governed by fastener limit states, and in each series of testing, the board behaved rigidly up until peak load.

Since numerical simulations and resultant design predictions in the previous sections are limited to a wall aspect ratio (*h*:*w*) of 2:1, wall aspect ratios higher than 2:1 and lower than 2:1 are simulated to validate the recommended shear design capacities. FCB and SG sheathing material properties and thicknesses are maintained. Wall configuration and aspect ratios are adopted from Liu et al. [4], are illustrated in Fig. 13 and are as follows:

- Two wall geometries: 1.22 m × 2.74 m (4 ft × 9 ft) and 2.44 m × 2.74 m (8 ft × 9 ft) with aspect ratios of 2.25:1 and 1.125:1, respectively.
- CFS studs have a web depth of 152.4 mm, flange width of 41.3 mm,

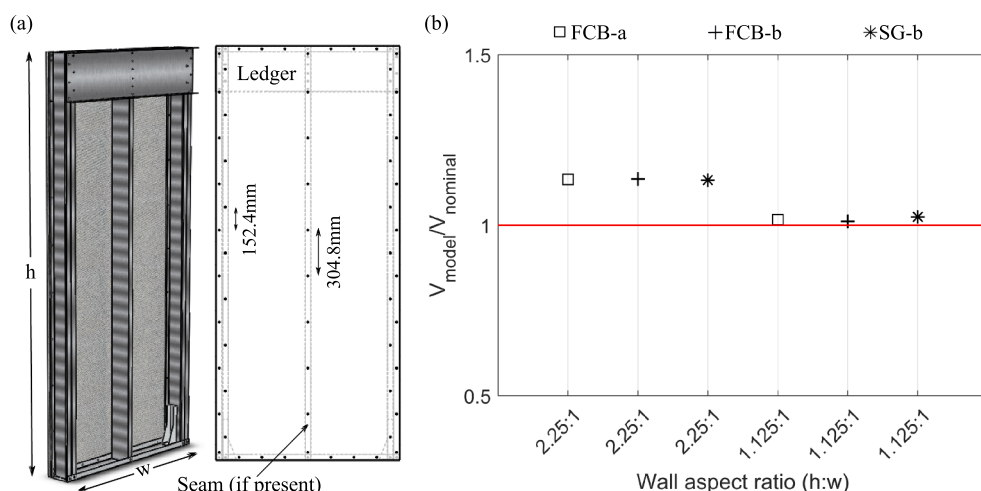


Fig. 13. CFS shear wall configuration for the different wall aspect ratios. (a) Schematic representation of FCB- and SG-sheathed CFS shear walls indicating the basic characteristics and basic additional structural details (ledger, vertical seam, staggered fasteners) of the walls. (b) Model-to-predicted ratios in varying aspect ratios (1.0 = perfect prediction).

lip depth of 12.7 mm and thickness of 1.37 mm (600S162-54 in [44]).

- CFS tracks have a web depth of 157.4 mm, flange width of 38.1 mm and thickness of 1.37 mm (600T150-54).
- S/HDU6 Simpson Strong-tie hold-down is used with a tensile stiffness of 2929 kN/m (56.7 kips/in.) and a compressive stiffness 1000 times higher.
- Perimeter fasteners between sheathing and studs are staggered at 152.4 mm (6 in.). Fasteners in the field stud are spaced at 304.8 mm (12 in.).
- A displacement of 0.127 m (5 in.) is monotonically applied.
- Both walls have a ledger (web: 304.8 mm, flange: 50.8 mm, thickness: 2.46 mm (1200T200-97)), and the 2.44 m × 2.74 m (8 ft × 9 ft) wall has a vertical panel seam. This manifests two lines of fasteners in the middle field stud spaced as at 152.4 mm (6 in.).

The finite element modeling lateral capacities of the two shear walls with different aspect ratios are compared to the recommended design capacities in Table 8 by using equations from AISI-S400 [1]. AISI-S400-15 [1] predicts the base shear capacity V_n through Eq. (5) for wall aspect ratios lower and equal to 2 ($h:w \leq 2$) and through Eq. (6) for wall aspect ratios higher than 2 and less or equal to 4 ($2 < h:w \leq 4$).

$$V_n = v_n w \quad (5)$$

$$V_n = v_n w (2w/h) \quad (6)$$

The results are illustrated in Fig. 13. The horizontal line represents perfect predictions at $V_{model}/V_{AISI} = 1$. For wall aspect ratios equal or less to 2:1, the prescriptive method accurately predicts shear strength, while for an aspect ratio higher than 2:1 the recommended values conservatively underpredict the strength of the wall by 14%-17%. In this case, the conservatism can be attributed to the presence of 304.8 mm (1 ft) deep ledger at the interior of the wall, which leads to a wall behavior similar to 1.22 m × 2.44 m (4 ft × 8 ft) ($h:w = 2:1$) instead of 1.22 m × 2.74 m (4 ft × 9 ft) ($h:w = 2.25:1$), as discussed in the relevant experimental study by Liu et al. [4].

6. Conclusions

This paper presents a thorough study of the lateral performance of FCB- and SG-sheathed CFS shear walls through a connection-level experimental program, a hysteretic parameter characterization, and a benchmark shear wall computational model.

Firstly, the shear response of the connections between cold-formed steel members and innovative types of sheathing such as fiber cement board (FCB) and steel-gypsum (SG) composite board is evaluated through an experimental program of 18 specimens under monotonic and cyclic loading. The results show that the connection capacity does not significantly vary between the two different screw types examined herein. Shear strength of CFS-to-SG connections is higher in comparison to CFS-to-FCB connection response in both monotonic and cyclic testing. The same is true for stiffness.

From this, connection backbones and Pinching4 hysteretic parameters are extracted. These parameters are intended to be used in future reduced-order or high fidelity finite element modeling of shear walls sheathed with FCB and SG composite sheathing under cyclic loading.

A benchmark fastener-based CFS shear wall computational modeling approach is implemented which accurately captures the lateral response of walls sheathed with FCB and SG sheathing. Modeling results highlight the contribution of connection-level response in subsystem behavior. Furthermore, failure mode is largely dependent on fastener spacing and sheathing rigidity.

Based on the finite element modeling shear wall results, design shear capacities per unit width for CFS shear walls are provided. While the modeling method implemented herein has been validated using full-scale experimental tests for OSB-sheathed shear walls, further testing of FCB- and SG-sheathed shear walls is needed for implementation into design specifications.

The finite element modeling program described herein is limited to monotonically loaded FCB- and SG-sheathed CFS shear walls. For modeling shear walls under cyclic loading, connection backbone response and full Pinching4 behavior are necessary in characterizing connection behavior. The Pinching4 uniaxial model can be used in phenomenological models, as well as in high fidelity simulations. These characterizations are provided to enable future work in either modeling approach.

7. Data availability statement

Some or all data, models, or code generated or used during the study are available from the corresponding author by request. The data include experimental raw data, and experimental and computational results.

CRediT authorship contribution statement

Fani Derveni: Conceptualization, Methodology, Software, Investigation, Visualization, Writing - original draft, Writing - review & editing. **Simos Gerasimidis:** Conceptualization, Methodology, Supervision, Writing - review & editing, Resources, Funding acquisition. **Kara D. Peterman:** Conceptualization, Methodology, Supervision, Writing - review & editing, Resources, Funding acquisition.

Declaration of Competing Interest

None.

Declaration of Competing Interest

The authors declare that they have no known competing financial interests or personal relationships that could have appeared to influence the work reported in this paper.

Acknowledgements

The authors would like to thank Dr. Benjamin W. Schafer and Dr. Tara C. Hutchinson for the discussions and feedback for this work within CFS-NHERI project. The authors would also like to acknowledge the lab technician at UMass Amherst, Mr. Mark Gauthier, for the lab support.

References

- [1] AISI-S400-15, North American standard for seismic design of cold-formed steel structural systems, in: AISI-S400, American Iron and Steel Institute, Washington, D.C.; 2015.
- [2] Serrette RL, Encalada J, Juadines M, Nguyen H. Static racking behavior of plywood, OSB, gypsum, and fiberbond walls with metal framing. *J Struct Eng* 1997;123(8):1079–86.
- [3] Branston AE, Chen CY, Boudreault FA, Rogers CA. Testing of light-gauge steel-frame - wood structural panel shear walls. *Can J Civ Eng* 2006;33(5):561–72. ISSN 03151468.
- [4] Liu P, Peterman KD, Schafer BW. Impact of construction details on OSB-sheathed cold-formed steel framed shear walls. *J Constr Steel Res* 2014;101:114–23.
- [5] Yu C. Shear resistance of cold-formed steel framed shear walls with 0.686 mm, 0.762 mm, and 0.838 mm steel sheet sheathing. *Eng Struct* 2010;32(6):1522–9.
- [6] DaBreo J, Balh N, Ong-Tone C, Rogers C. Steel sheathed cold-formed steel framed shear walls subjected to lateral and gravity loading. *Thin-Wall Struct* 2014;74:232–45.
- [7] Fülop L, Dubina D. Performance of wall-stud cold-formed shear panels under monotonic and cyclic loading: Part I: Experimental research. *Thin-Wall Struct* 2004;42(2):321–38.
- [8] Zhang W, Mahdavian M, Li Y, Yu C. Experiments and simulations of cold-formed steel wall assemblies using corrugated steel sheathing subjected to shear and gravity loads. *J Struct Eng* 2017;143(3):04016193.
- [9] Mohebbi S, Mirghaderi SR, Farahbod F, Sabbagh AB, Torabian S. Experiments on seismic behaviour of steel sheathed cold-formed steel shear walls cladded by gypsum and fiber cement boards. *Thin-Wall Struct* 2016;104:238–47.
- [10] Macillo V, Fiorino L, Landolfo R. Seismic response of CFS shear walls sheathed with nailed gypsum panels: Experimental tests. *Thin-Wall Struct* 2017;120:161–71.
- [11] Fiorino L, Macillo V, Landolfo R. Shake table tests of a full-scale two-story sheathing-braced cold-formed steel building. *Eng Struct* 2017;151:633–47.
- [12] Zeynalian M, Ronagh HR. Seismic performance of cold formed steel walls sheathed by fibre-cement board panels. *J Constr Steel Res* 2015;107:1–11.
- [13] Khaliq W, Moghis A. Shear capacity of cold-formed light-gauge steel framed shear-wall panels with fiber cement board sheathing. *Int J Steel Struct* 2017;17(4):1404–14.
- [14] Hoehler MS, Smith CM, Hutchinson TC, Wang X, Meacham BJ, Kamath P. Behavior of steel-sheathed shear walls subjected to seismic and fire loads. *Fire Saf J* 2017;91:524–31.
- [15] McKenna F, Fenves G, Jeremic B, Scott M. Open system for earthquake engineering simulation; 2000, URL <http://opensees.berkeley.edu>. [May 2008].
- [16] ABAQUS, Abaqus theory guide, in: Version 6.14, Dassault Systems Simulia Corp, USA; 2014.
- [17] Buonopane S, Bian G, Tun T, Schafer B. Computationally efficient fastener-based models of cold-formed steel shear walls with wood sheathing. *J Constr Steel Res* 2015;110:137–48.
- [18] Bian G, Padilla-Llano D, Leng J, Buonopane S, Moen C, Schafer B. OpenSees modeling of cold-formed steel framed wall system, in: Proceedings of 8th international conference on behavior of steel structures in seismic areas. 2015.
- [19] Ngo HH. Numerical and experimental studies of wood sheathed cold-formed steel framed shear walls M.S. thesis MD: Johns Hopkins University, Baltimore; 2014.
- [20] Ding C. Monotonic and Cyclic Simulation of Screw-Fastened Connections for Cold-Formed Steel Framing M.S. thesis VA: Virginia Tech, Blacksburg; 2015.
- [21] Derveni F, Gerasimidis S, Schafer BW, Peterman KD. High fidelity finite element modeling of wood-sheathed cold-formed steel shear walls. *J Struct Eng* 2020. [https://doi.org/10.1061/\(ASCE\)ST.1943-541X.0002879](https://doi.org/10.1061/(ASCE)ST.1943-541X.0002879). Forthcoming.
- [22] Singh A, Hutchinson TC. Finite element modeling and validation of steel-sheathed cold-formed steel framed shear walls. In: Proceedings of the International Specialty Conference on Cold-Formed Steel Structures. St. Louis, Missouri; 2018.
- [23] Zhang Z, Schafer BW. Simulation of steel sheet sheathed cold-formed steel framed shear walls. In: Proceedings of the Annual Proceedings of the Annual Stability Conference Structural Stability Research Council April 2–5. St. Louis, Missouri; 2019.
- [24] Fiorino L, Shakeel S, Macillo V, Landolfo R. Seismic response of CFS shear walls sheathed with nailed gypsum panels: Numerical modelling. *Thin-Wall Struct* 2018;122:359–70.
- [25] Peterman KD, Nakata N, Schafer BW. Hysteretic characterization of cold-formed steel stud-to-sheathing connections. *J Constr Steel Res* 2014;101:254–64.
- [26] Tao F, Chatterjee A, Moen CD. Monotonic and cyclic response of single shear cold-formed steel-to-steel and sheathing-to-steel connections, Report. No. CE/VPI-ST-16-01, Virginia Tech., Blacksburg, Virginia; 2017.
- [27] Vieira L, Schafer BW. Experimental results for translational stiffness of stud-sheathing assemblies, AISI-COFS Project on Sheathing Braced Design of Wall Studs.
- [28] Selvaraj S, Madhavan M. Investigation on sheathing-fastener connection failures in cold-formed steel wall panels. *Structures*, vol. 20. Elsevier; 2019. p. 176–88.
- [29] Fiorino L, Pali T, Bucciero B, Macillo V, Terracciano MT, Landolfo R. Experimental study on screwed connections for sheathed CFS structures with gypsum or cement based panels. *Thin-Wall Struct* 2017;116:234–49.
- [30] Green GG, Winter G, Cuykendall TR. Light gage steel columns in wall-braced panels. Cornell Univ.; 1947.
- [31] Winter G. Lateral bracing of beams and columns, ASCE Transactions, Paper (3044).
- [32] AISI-S100-16, North American Specification for the Design of Cold-Formed Steel Structural Members. In: AISI-S100, American Iron and Steel Institute, Washington, D.C.; 2016.
- [33] Krawinkler H, Parisi F, Ibarra L, Ayoub A, Medina R. Development of a testing protocol for wood frame structures, CUREE Publication No, W-02, California.
- [34] Okasha AF. Performance of steel frame/ wood sheathing screw connections subjected to monotonic and cyclic loading, M.Eng. thesis, McGill University, Montreal, Canada; 2004.
- [35] Fiorino L, Della Corte G, Landolfo R. Experimental tests on typical screw connections for cold-formed steel housing. *Eng Struct* 2007;29(8):1761–73.
- [36] Fiorino L, Macillo V, Landolfo R. Experimental characterization of quick mechanical connecting systems for cold-formed steel structures. *Adv Struct Eng* 2017;20(7):1098–110.
- [37] Lowes L, Mitra N, Altoontash A. A beam-column joint model for simulating the earthquake response of reinforced concrete frames, PEER Report 2003/10, Pacific Earthquake Engineering Research Center, University of California, Berkeley.
- [38] Altoontash A. Simulation and damage models for performance assessment of reinforced concrete beam-column joints Ph.D. thesis California: Stanford university Stanford; 2004.
- [39] MATLAB, The MathWorks Inc., Natick, Massachusetts; 2019.
- [40] Branston AE. Development of a Design Methodology for Steel Frame/Wood Panel Shear Walls M.Eng. thesis Montreal, Canada: McGill University; 2004.
- [41] Gypsum Association, Gypsum board typical mechanical and physical properties, GA 235 10.
- [42] Simpson Strong-Tie Co., Inc., Light Gauge Steel Construction Connectors, Dublin, CA, USA.
- [43] Leng J, Schafer BW, Buonopane SG. Modeling the seismic response of cold-formed steel framed buildings: model development for the CFS-NEES building. *Proceedings of the annual stability conference-structural stability research council*. 2013.
- [44] AISI-S200-12, North American Specification for Cold-formed steel framing - General Provisions, in: AISI-S200, American Iron and Steel Institute, Washington, D.C.; 2012.